

Transparent Josephson Junctions in Higher-Order Topological Insulator WTe_2 via Pd Diffusion

Martin Endres,^{1,*} Artem Kononov,¹ Michael Stiefel,² Marcus Wyss,³ Hasitha Suriya Arachchige,⁴ Jiaqiang Yan,^{4,5} David Mandrus,^{6,4,5} Kenji Watanabe,⁷ Takashi Taniguchi,⁷ and Christian Schöenberger^{1,3,†}

¹*Department of Physics, University of Basel, Klingelbergstrasse 82, 4056 Basel, Switzerland*

²*Laboratory for Nanoscale Material Science, Swiss Federal Laboratories for Material Science and Technology, EMPA, Überlandstrasse 129, 8600 Dübendorf, Switzerland*

³*Swiss Nanoscience Institute, University of Basel, Klingelbergstrasse 82, 4056 Basel, Switzerland*

⁴*Department of Physics and Astronomy, University of Tennessee, Knoxville, Tennessee 37996, USA*

⁵*Material Science and Technology Division, Oak Ridge Laboratory, Oak Ridge, Tennessee 37831, USA*

⁶*Department of Materials Science and Engineering,*

University of Tennessee, Knoxville, Tennessee 37996, USA

⁷*National Institute for Materials Science, 1-1 Namiki, Tsukuba 305-0044, Japan*

(Dated: August 22, 2022)

Highly transparent superconducting contacts to a topological insulator (TI) remain a persistent challenge on the route to engineer topological superconductivity. Recently, the higher-order TI WTe_2 was shown to turn superconducting when placed on palladium (Pd) bottom contacts, demonstrating a promising material system in pursuing this goal. Here, we report the diffusion of Pd into WTe_2 and the formation of superconducting $PdTe_x$ as the origin of observed superconductivity. We find an atomically sharp interface in vertical direction to the van der Waals layers between the diffusion crystal and its host crystal, forming state-of-the-art superconducting contacts to a TI. The diffusion is discovered to be non-uniform along the width of the WTe_2 crystal, with a greater extend along the edges compared to the bulk. The potential of this contacting method is highlighted in transport measurements on Josephson junctions by employing external superconducting leads.

I. INTRODUCTION

Topological insulators (TI) are insulating in the bulk while hosting gap-less boundary states in which the spin of the electron is locked to its momentum [1]. When brought in contact with a s-wave superconductor, a novel pairing mechanism is predicted with Cooper pairs that resemble an effectively spin-less superconductor [2, 3]. Such topological superconductors could host Majorana bound states, the elementary building block of fault-tolerant quantum bits [4].

Fundamental to this approach is a highly transparent interface between the superconductor and topological insulator [5] through which the boundary states are proximitized. Even with state-of-the-art nano-fabrication it remains challenging to create such pristine material interfaces as oxidation [6–9], contamination and rough crystal interfaces introduce defects and therefore decrease contact transparency [10].

The van der Waals (vdW) material WTe_2 is predicted to be a higher-order TI [11–15], hosting topological edge states at its crystal hinges. It was recently shown that thin crystals of the material placed on top of palladium (Pd) bottom contacts turn superconducting [16], with a pronounced flow of super-current along the edges of a Josephson junction (JJ) formed out of this material system [17].

Here, we report diffusion of Pd into the WTe_2 forming superconducting $PdTe_x$ as the origin of superconductivity

in the WTe_2 /Pd system. The interface between $PdTe_x$ and WTe_2 in vertical direction to the vdW layers is found to be atomically sharp, eliminating crystal-roughness between the superconductor and the higher-order TI completely. We further investigate the formation of $PdTe_x$ along the width of the WTe_2 host crystal and find it to be non-uniform, with greater extend along the edges compared to the bulk. The potential of this novel contacting method to WTe_2 is highlighted in transport measurements on JJs that show improved quality when contacted externally by an intrinsic superconductor.

II. PD DIFFUSION IN WTe_2

We begin with describing the general structure of WTe_2 Josephson junctions formed with Pd. Fabrication starts with patterning parallel lines of Pd on p-doped Si substrates with 285 nm SiO_2 on top. Next, the vdW materials hexagonal boron nitride (hBN) and WTe_2 are exfoliated and afterwards stacked on top of the Pd bottom contacts, using a standard dry pick-up technique [18]. Until full encapsulation with hBN, WTe_2 is handled inside an inert glovebox-atmosphere to protect the material from oxidation [6–8]. After the stacking process, the polymer stamp is separated from the stacked device by heating the sample to 155 °C for ≈ 10 min. The remaining polymer residues are chemically dissolved afterwards. Depending on the desired transport experiment, contact to WTe_2 is made either through the Pd bottom contacts or by etching through the covering top hBN and depositing superconducting contacts from the top. It should be

* martin.endres@unibas.ch

† christian.schoenberger@unibas.ch

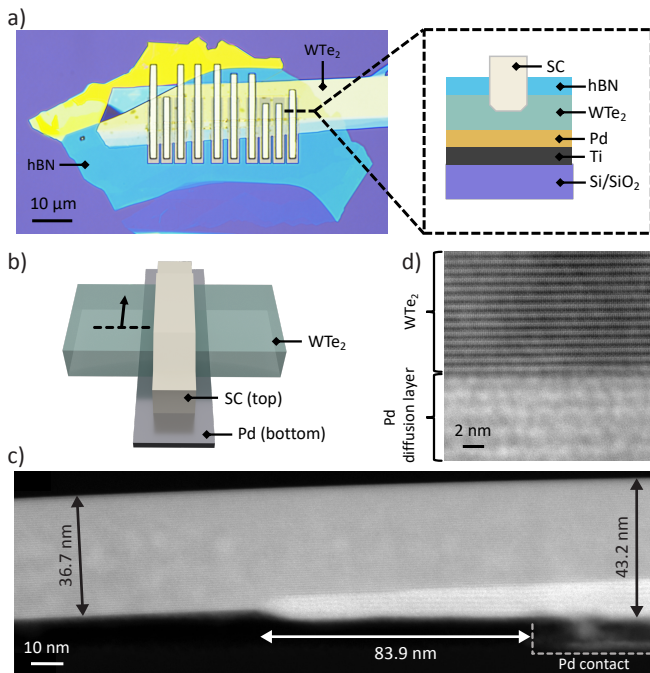


FIG. 1. **Pd diffusion inside the WTe_2 crystal.** a) Left: optical image of the elongated WTe_2 flake, covered with hBN on top of Pd contacts, with additional superconducting contacts (niobium) on top. Right: a schematic cross section of the device in a region of single Pd contact. b) Illustration of the WTe_2 crystal on a single Pd bottom contact including a superconducting edge contact from the top. The direction of the cut lamella for the STEM image is indicated by the dashed line, the viewing direction of the image by the arrow. c) High resolution STEM image taken at the edge of the Pd bottom contact (indicated by grey dashed line at the bottom right). A bright diffusion layer at the interface between the Pd bottom contact and the WTe_2 crystal has formed. Black arrows indicate the thickness of the WTe_2 crystal, the white arrow shows the lateral extent of diffusion in WTe_2 from the edge of the original Pd contact. d) Zoom-in STEM image of the interface between the WTe_2 crystal and the diffusion layer.

noted, that superconductivity is induced into WTe_2 by the Pd contacts alone [16, 17] and that additional superconducting contacts are not required to form Josephson junctions. Fig. 1 a) demonstrates an optical image of one of the devices. This device was prepared specially for electron microscopy, so additional top superconducting contacts do not have any practical purpose and are placed to replicate real transport devices. An extended description of the fabrication process can be found in the supplementary materials [19–21].

In order to investigate the origin of superconductivity in WTe_2 in contact with Pd, we conduct high resolution scanning transmission electron microscopy (STEM) imaging of the interface region. The illustration in Fig. 1 b) indicates the direction of the extracted lamella by a dashed line and the viewing direction by a perpendicular arrow. Fig. 1 c) presents the STEM image taken with a high-annular angular dark field detector

(HAADF) at the edge of a Pd bottom contact, reaching into the weak link of the junction. Visible at first glance is a bright layer, that has formed at the interface between the Pd bottom contact and the WTe_2 crystal on top. Moreover, the original Pd contact in the bottom right corner of the Fig. 1 c) appears hollow and faded out, suggesting that the bright layer in WTe_2 is a result of Pd diffusion from the contact.

The presence of the diffusion layer in WTe_2 creates a pronounced swelling of the crystal, as highlighted by two thickness measurements of the WTe_2 flake in Fig. 1 c): inside the junction and on top of the Pd bottom contact. For pristine WTe_2 we extract an inter-layer spacing of $c \sim 7.4 \text{ \AA}$ that agrees with the literature value [22, 23]. Inside the diffusion layer the perceived layer spacing has doubled to $c \sim 14.8 \text{ \AA}$. We connect the change in the layer spacing with the formation of a new crystal structure at the interface of WTe_2 and Pd, rather than merely intercalation of the original crystal by Pd. The formation of a new structure is further supported by fig. 1 d), where we see, that the transition between the newly formed crystal and WTe_2 is very sharp and takes place on a single layer scale. We also would like to note, that the diffusion forming the new structure is quite anisotropic. Laterally, along the vdW layers, the diffusion layer extends $\sim 84 \text{ nm}$ while vertically, perpendicular to the vdW layers, it only reaches $\sim 16 \text{ nm}$ at its maximum. The lateral diffusion inside the JJ can diminish the length of the JJ, which could be especially prominent for the shorter junctions.

In the next section we analyze the atomic composition of the diffusion layer using energy dispersive x-ray (EDX) analysis. Fig. 2 a) on the left shows a STEM image taken at the position of a superconducting niobium (Nb) top-contact in this device. For better orientation, the location is illustrated in b). From the bottom to the top, the faded Pd bottom contact, the Pd diffusion layer adjacent to the pristine WTe_2 crystal and the Nb top contact are visible. Towards the right, EDX spectra of the elements in this slab are shown. Nb (turquoise) and the sticking layer for the Pd bottom contacts, titanium (Ti) are at their expected positions. Qualitatively, the concentration of tungsten (W) and tellurium (Te), represented in red and orange, respectively, are maximal in the unchanged WTe_2 crystal but reduced in the diffusion layer. Pd (in blue) has diffused through the entire WTe_2 crystal and is the dominating element inside the structurally changed layer. The concentration of Pd at the position of the original bottom contact is diminished, suggesting that depletion of the available material stopped the further growth of the diffusion layer.

A quantitative analysis of the crystal composition is shown in Fig. 2 b), following a trace indicated by the red arrow in the STEM image in a). The ratio of W:Te is $\sim 1:2$ and remains the same throughout most of the thickness. For Pd, two distinct concentration levels are visible, a high level $\sim 60\%$ that coincides with the structurally changed lattice and a second, low level $\sim 20\%$ inside the preserved WTe_2 crystal. The ratio of Pd:Te $\sim 3:1$ suggests that the diffusion layer is not one of the

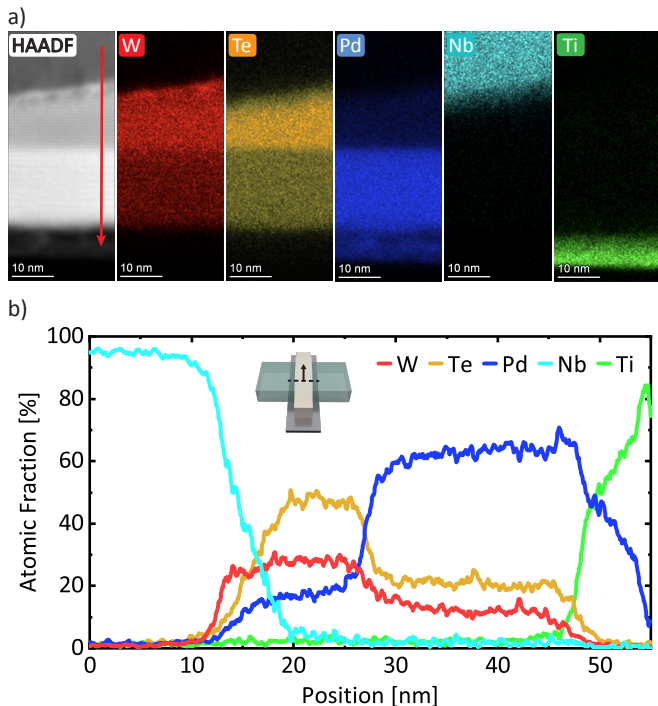


FIG. 2. **EDX analysis of the Pd diffusion.** a) STEM image with the direction of the line cut in b) indicated by a red arrow. Presented towards the right is the EDX analysis with elements existing in the device. Moving from the bottom to the top, the Pd bottom contact is followed by highly Pd interspersed WTe_2 layer that has structurally changed. Above, the crystal transitions sharply into the original crystal structure. b) EDX line cut along the direction indicated in a), with the position of the investigated lamella marked in the insert. Pd has diffused in vertical direction through the entire WTe_2 crystal, with a sharp concentration increase in the structurally changed area that coincides with the STEM image.

known superconductors PdTe or PdTe_2 [24–27]. In the unchanged WTe_2 crystal above, Pd likely intercalates the vdW layers. So possibly, a threshold concentration of Pd is required to trigger the crystallographic change, such that the vertical extend of the diffusion layer is determined by the interplay of available Pd and thermal activation energy. The remaining Pd concentration above the PdTe_x layer quickly decays in direction parallel to the vdW layers and extends ~ 50 nm laterally beyond the structurally changed diffusion layer, as shown in [19].

III. DIFFUSION ALONG THE EDGES

Further, we investigate the uniformity of the PdTe_x diffusion layer along the width of the Josephson junction. For this, we have analysed several lamellas that are oriented perpendicular to the direction of current in the JJ. The regions near the physical edges of WTe_2 are of particular interest, since additional Pd is available there due to the Pd bottom contacts extending beyond the crystal.

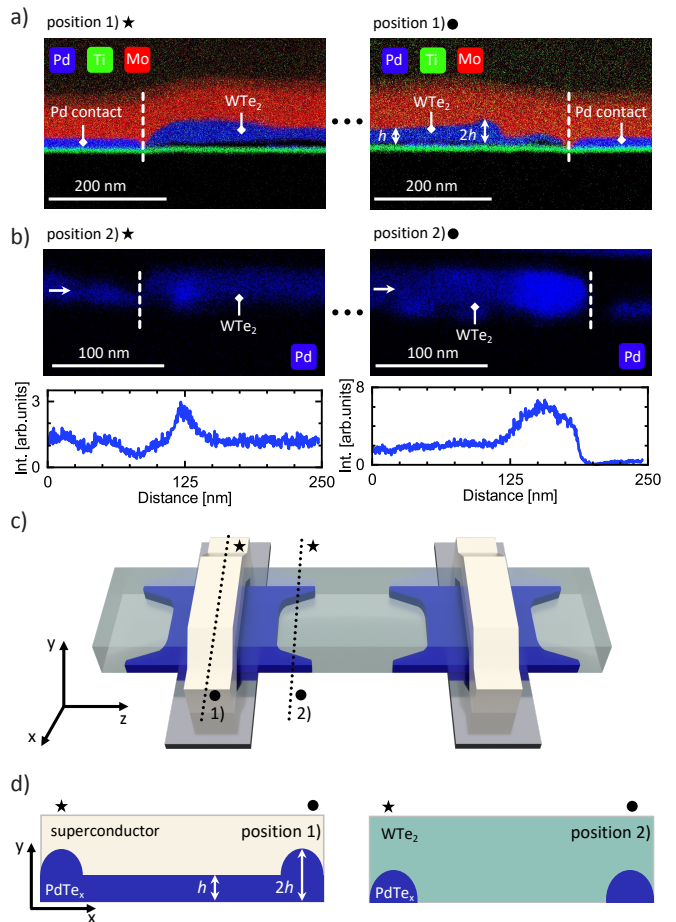


FIG. 3. **Enhanced Pd diffusion along the edges of the WTe_2 crystal.** a) EDX analysis of a cross section taken on the Pd contact along position 1), as indicated in the schematics in c). The given sample was equipped with a superconducting MoRe contact, evidenced by the Mo EDX signal in red. The left and right image correspond to the crystal edges marked by \star and \bullet in the schematics, respectively. Visible is the swelling of WTe_2 to a thickness $\sim 2h$ at the edge, compared to the bulk thickness $\sim h$, indicated in the right image. b) EDX signal and extracted intensity (Int.) profile taken towards the inside of the junction, indicated by position 2) in c). The left and right image correspond to positions \star and \bullet of the WTe_2 crystal, respectively. Visible in the EDX data is an increased intensity of the Pd signal at the edges of the crystal compared to the bulk. The increased Pd concentration is as well visible by the enhanced EDX signal in the line cuts taken along the direction pointed out by the horizontal arrow. c) Illustration of the inhomogeneous diffusion profile of PdTe_x inside the WTe_2 host crystal. The self-formed PdTe_x layer is drawn in blue inside the host crystal. d) Cross sectional cuts through the illustration along positions 1) and 2) in c). The edges are marked by \star and \bullet for orientation.

The first lamella was cut out through the middle of the bottom Pd contact in a sample with additional, this time molybdenum-rhenium (MoRe), top contacts, as illustrated by position 1) in Fig. 3 c). Fig. 3 a) presents two EDX spectra obtained at the two edges marked by \star and \bullet in the previous illustration. Outside of the WTe_2

flake we observe a layer of Pd with uniform thickness sandwiched between the MoRe top- and Ti bottom-layer. Interestingly, inside WTe_2 near the edges, the thickness h of the PdTe_x diffusion layer increases within a region of ~ 100 nm away from the edge, as marked in the right spectrum of Fig. 3 a). Further from the edges, Pd is evenly distributed throughout the WTe_2 crystal. The difference of PdTe_x thickness on the edges and in the middle of WTe_2 reaches a factor of ~ 2 .

The increase in thickness of PdTe_x near the edges can be intuitively explained taking into account the fabrication procedure. During the last step of stacking, when the substrate is heated up to 155°C to release the hBN/ WTe_2 stack, the formation of the PdTe_x takes place. In WTe_2 far away from the edges this process stops before reaching the full thickness of the flake due to depletion of available Pd. Near the edges, due to availability of additional Pd, this process continues potentially even through the whole thickness of WTe_2 . Afterwards, the top WTe_2 layers, not transformed to PdTe_x , are etched away during CHF_3/O_2 plasma etching of hBN prior to the deposition of the superconductor. This explanation is further corroborated by the uniform Pd concentration in Fig. 3 a) in contrast with the step in concentration in Fig. 2 b).

The increased Pd availability on the edges of the WTe_2 has the potential not only to increase the PdTe_x thickness, but also to provide further diffusion inside the Josephson junction. To check this, we made a second lamella from another sample, which is cut inside the Josephson junction close to the end of Pd bottom contact, as shown as position 2) in Fig. 3 c). Visible in the EDX spectrum in Fig. 3 b) is an elevated intensity of Pd compared to the bulk at both ends of the crystal, highlighted by line cuts through the spectra along the horizontal arrows. This indicates, that PdTe_x is indeed penetrating further inside the junction along the edges of WTe_2 as visualized in Fig. 3 c).

We can roughly estimate the extent of the PdTe_x diffusion along the edges. Assuming that an increase by a factor of 2 in thickness h of PdTe_x on the edges, as compared to the bulk (see Fig. 3 d)), yields the same increase in the diffusion inside the JJ along the edge. Taking from fig. 1 c), that the PdTe_x layer extends ~ 85 nm inside the junction in the bulk, we would expect it to extend ~ 170 nm along the edges. This diffusion could generate signatures of ‘artificial’ edge supercurrents not due to a topological state. Nonetheless, evidence of topological hinge states in WTe_2 has been observed in combination with superconducting niobium contacts [15, 28], where no edge diffusion is expected.

IV. JOSEPHSON JUNCTION WITH FULLY SUPERCONDUCTING CONTACTS

During the formation of PdTe_x in WTe_2 the majority of the Pd from the bottom contacts is depleted (see Fig. 1-3), thus creating a low quality interface between

bottom contacts and the newly formed Josephson junction. In this section we demonstrate a method to harness the full potential of the high quality Josephson junction formed in WTe_2 with Pd diffusion by employing additional superconducting contacts from the top.

The fabrication process follows the description in section II. After obtaining the stack, superconducting leads are patterned via standard e-beam lithography and sputtered onto the sample after etching through the top hBN with CHF_3/O_2 plasma. Prior to the deposition of MoRe superconducting leads, we perform a short Ar milling inside the sputtering chamber to remove the oxide layer from WTe_2 . In order to avoid degradation of the JJs due to etching, the superconducting top contacts are separated by a distance $l_{Pd} \sim 0.5 \mu\text{m}$ from the edge of the Pd bottom contacts, as indicated in the schematics in Fig. 4 a). Fig. 4 a) shows a finished device with top MoRe leads and its fabricated layer sequence to the right.

Measurement of the device is performed in a quasi four-terminal setup, illustrated in Fig. 4 a). In this configuration, the measured differential resistance includes the contribution from the Josephson junction and the resistances of the interfaces between the MoRe and superconducting PdTe_x , but excludes the line resistances in the cryostat. Fig. 4 b) and c) show the $dV/dI(I)$ and $V(I)$ dependencies, measured on a $1 \mu\text{m}$ long Josephson junction, with their behavior being representative for a number of samples we have studied. The curves reveal several abrupt transitions with current. Steps at $I \sim \pm 11 \mu\text{A}$ have minimal hysteresis and correspond to the switching of superconducting PdTe_x to the normal state or alternatively to a Josephson junction that has potentially formed at the interface of the vdW stack with MoRe [29].

The observed vanishing resistance at low bias currents by itself is not sufficient to ensure that the fabricated device performs indeed as a JJ. Potentially, the inhomogeneous diffusion of PdTe_x could lead to a closed superconducting path through the weak link. In order to rule out this option, we study the dependence of dV/dI on the bias current I and perpendicular magnetic field B , as shown in Figure 4 d). Visible is a periodic ‘Fraunhofer’-like interference pattern that is a key signature of the Josephson effect. The oscillation periodicity $\delta B = 0.13 \text{ mT}$ is connected to a flux quantum Φ_0 threading the effective junction area $A_{eff} = w \times \ell_{eff}$, with $w = 4.3 \mu\text{m}$ being the width of the junction and ℓ_{eff} being the effective length. The calculated $\ell_{eff} \sim 3.8 \mu\text{m}$ exceeds the physical junction length of $\sim 1 \mu\text{m}$. However, it can be explained by the contact geometry, assuming that half of the magnetic flux through the superconducting contacts is screened into the junction [30]. Additionally, a close look at the amplitude of consecutive lobes reveals a non-monotonous behavior, reminiscent of an even-odd effect. A non-sinusoidal current phase relation of the junction [17] or an inhomogeneous current distribution [30], originating from the diffusion profile of PdTe_x , can create this feature.

Having established the Josephson effect through WTe_2 , we take a closer look at the lower current behavior ob-

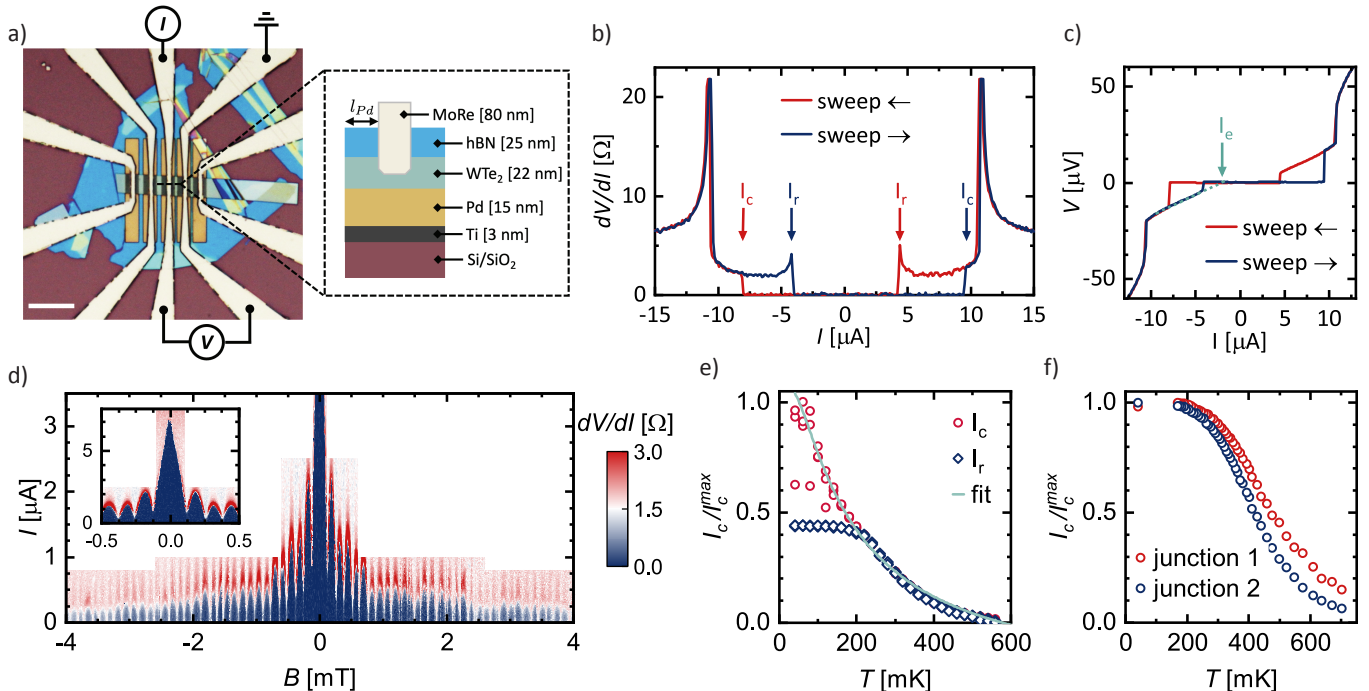


FIG. 4. **Switching characteristics of Josephson junctions with superconducting or normal leads.** a) Optical image of the device with an illustration of the quasi four-terminal measurement setup. The fabricated layer sequence is shown on the right. Scale bar is 10 μm. b) dV/dI curves at zero magnetic field of a JJ with superconducting contacts for two different sweep directions of the bias current. The hysteretic switching current depending on the sweep direction is visible from the shift of the critical current I_c and the re-trapping current I_r . c) $V(I)$ curves corresponding to the data in b). The excess current I_e is evaluated from the intersection of the extended $V(I)$ curve to zero voltage. d) dV/dI as a function of bias current I and perpendicular magnetic field B , following the ‘Fraunhofer’ pattern expected for a Josephson junction. The insert shows the full range of the central lobe around $B = 0$. e) Temperature dependence of the switching and re-trapping currents I_c and I_r , respectively, of the same device as in b). The data $I_c(T)$ is fitted in the scope of a diffusive long junction, plotted in light green. f) Switching current I_c as a function of temperature T for two different JJs that are contacted only through Pd bottom contacts.

served in fig. 4 b) and c). First, in the superconducting branch of the JJ, the differential resistance is zero, implying that there is no measurable contribution of the MoRe/PdTe_x interfaces. Second, in contrast to the previously studied devices with solely Pd leads [17], the switching behavior is highly hysteretic. The transition from the superconducting to the resistive branch, denoted by the switching current I_c , takes place at higher absolute current values than the transition in opposite sweep direction, denoted by the re-trapping current I_r , highlighted in Fig. 4 b).

Even though the hysteretic switching of the Josephson junction is most commonly explained by the junction being in the underdamped regime [31], we would argue that in our case overheating [32, 33] plays the dominating role. Starting from the superconducting branch, no heat is dissipated in the Josephson junction before switching to the resistive branch. In contrast, lowering the bias current from the resistive branch includes dissipation of heat in the normal weak link, leading to a higher electron temperature. This explanation is corroborated by the temperature dependence of I_c and I_r shown in Fig. 4 e). Moving from high towards low temperatures, I_c and I_r

both increase continuously down to $T \sim 220$ mK, when I_r begins to saturate while I_c remains increasing. Furthermore, this explanation is additionally supported by the devices with only Pd contacts. There, due to the normal Pd contacts remaining dissipative at all times, I_c saturates at low temperatures, as shown in Fig. 4 f).

Next, we characterize the quality of the PdTe_x/WTe₂ interface. Compared to conventional superconducting contacts to WTe₂, the Josephson effect in junctions formed by Pd interdiffusion is found to be more robust in terms of junction length and magnetic field resilience [17]. Additionally, due to reduced heating effects, the here proposed devices support a critical current density twice as large compared to conventional contacts [28] at four times the junction length. The 1 μm long junction presented in fig. 4 b) maintains the Josephson effect with a critical current density j_c of up to $j_c > 10^8$ A m⁻² while comparable junctions with even a shorter length up to 230 nm and conventional superconducting contacts are found to be limited by $j_c \sim 1 \times 10^7$ A m⁻² - 5×10^7 A m⁻² [28].

Further, from fig. 4 e) we see that I_c is suppressed at 0.6 K, which is lower than the critical temperature $T_c = 1.2$ K [34] of the formed PdTe_x. We connect this

reduction with the great length of the junction and fit for this reason $I_c(T)$ with an expression for a long diffusive junction [32, 35]

$$I_c = \eta \frac{aE_{Th}}{eR_N} \left[1 - b \exp\left(\frac{-aE_{th}}{3.2k_B T}\right) \right]. \quad (1)$$

Here, a and b are constants equal to 10.82 and 1.30, respectively, k_B the Boltzmann constant and E_{Th} the Thouless energy. The empirical pre-factor $\eta \in [0, 1]$ can be interpreted as a measure for the interface quality, scaling the maximum I_c . The data in fig. 4 e) is well described by the model which yields $\eta = 0.5$ and $E_{Th} = 3.87 \mu\text{eV}$. A similar fit procedure for the data in fig. 4 f), obtained from a junction with only Pd contacts, is not reliable as $I_c(T < 400 \text{ mK})$ is limited by heating effects and deviates strongly from the theoretical prediction.

The evaluation of the interface transparency is corroborated by the excess current I_e , extracted from the $V(I)$ curve in fig. 4 c). We extrapolate I_e after the transition from the superconducting to the resistive branch and obtain [36] $I_e R_N / \Delta \sim 0.03$, using $\Delta = 1.76 k_B T_c = 182 \mu\text{eV}$ [34]. In the framework of Octavio-Tinkham-Blonder-Klapwijk theory [37, 38], this relates to a junction transparency $T = 1/(1 + Z^2) \sim 0.5$, with $Z \sim 1.1$.

At this point we would like to comment on the role of R_N in the two analytical models of the preceding analysis yielding a transparency ~ 0.5 . The bulk conductivity of WTe_2 increases with flake thickness [39]. These additional bulk modes in the normal state shunt R_N , but do not participate in superconducting transport of the long junction due to their fast decay $I_{c,bulk} \propto \ell_{mfp}^2 / L_w^3$, compared to ballistic edge modes $I_{c,edge} \propto 1/L_w$ [40], with ℓ_{mfp} being the electronic mean free path. This phenomenon has also been reported in JJs formed of the topological material Bi_2Se_3 [41]. The extracted transparency is therefore systematically underestimated and serves only as a lower bound to the real value.

V. CONCLUSION

We have demonstrated a robust method to form atomically sharp superconducting contacts to WTe_2 mediated by Pd diffusion during stacking. Josephson junctions formed by these contacts are highly transparent. Given recent reports of similar processes in BiSbTe [36, 42] this method could be a promising approach for other topological candidates based on Te compounds. We have further demonstrated that the diffusion inside the host crystal could be non-uniform, generating false signatures of superconducting edge currents. Therefore, caution has to be exercised in the evaluation of diffusion driven Josephson junctions, when assigning it to topological superconductor. Furthermore, we proposed a method to avoid

overheating in transport through Pd diffusion mediated Josephson junctions by employing additionally superconducting leads.

Note. During the preparation of this manuscript we became aware of a recent publication [43], which also demonstrates the interdiffusion of Pd into WTe_2 with the formation of PdTe leading to superconductivity.

ACKNOWLEDGMENTS

We thank Paritosh Karnatak for fruitful discussions. This project has received funding from the European Research Council (ERC) under the European Union's Horizon 2020 research and innovation programme: grant agreement No 787414 TopSupra, by the Swiss National Science Foundation through the National Centre of Competence in Research Quantum Science and Technology (QSIT), and by the Swiss Nanoscience Institute (SNI). A.K. was supported by the Georg H. Endress foundation. D.G.M. and J.Y. acknowledge support from the U.S. Department of Energy (U.S.-DOE), Office of Science - Basic Energy Sciences (BES), Materials Sciences and Engineering Division. H.S.A. was supported by the Gordon and Betty Moore Foundation's EPiQS Initiative through Grant GBMF9096 and the Shull Wollan Center Graduate Research Fellowship. D.G.M. acknowledges support from the Gordon and Betty Moore Foundation's EPiQS Initiative, Grant GBMF9069. K.W. and T.T. acknowledge support from the Elemental Strategy Initiative conducted by MEXT, Japan and the CREST (JP-MJCR15F3), JST.

AUTHOR CONTRIBUTIONS

M.E. has fabricated the devices. M.E. and A.K. measured the devices in transport. M.S. and M.W. performed the STEM and EDX imaging. H.S.A., J.Y. and D.G.M. provided the WTe_2 crystals. K.W., T.T. provided hBN crystals. M.E., A.K. and C.S. analysed the data and wrote the manuscript.

COMPETING INTERESTS

The authors declare no competing interest.

DATA AVAILABILITY

All data in this publication are available in numerical form in the Zenodo repository at <https://doi.org/10.5281/zenodo.6556998>.

[1] L. Fu and C. L. Kane, Topological insulators with inversion symmetry, *Phys. Rev. B* **76**, 045302 (2007).

[2] L. Fu and C. L. Kane, Superconducting proximity effect and majorana fermions at the surface of a topological

- insulator, *Physical Review Letters* **100**, 096407 (2008).
- [3] C. W. Beenakker, Search for majorana fermions in superconductors, *Annual Review of Condensed Matter Physics* **4**, 113 (2013).
- [4] T. Hyart, B. Van Heck, I. C. Fulga, M. Burrello, A. R. Akhmerov, and C. W. Beenakker, Flux-controlled quantum computation with Majorana fermions, *Physical Review B - Condensed Matter and Materials Physics* **88**, 35121 (2013).
- [5] P. Schüffelgen, D. Rosenbach, C. Li, T. W. Schmitt, M. Schleenvoigt, A. R. Jalil, S. Schmitt, J. Kölzer, M. Wang, B. Bennemann, U. Parlak, L. Kibkalo, S. Trelenkamp, T. Grap, D. Meertens, M. Luysberg, G. Musler, E. Berenschot, N. Tas, A. A. Golubov, A. Brinkman, T. Schäpers, and D. Grützmacher, Selective area growth and stencil lithography for in situ fabricated quantum devices, *Nature Nanotechnology* **14**, 825 (2019).
- [6] F. Ye, J. Lee, J. Hu, Z. Mao, J. Wei, and P. X.-L. Feng, Environmental Instability and Degradation of Single- and Few-Layer WTe₂ Nanosheets in Ambient Conditions, *Small* **12**, 5802 (2016).
- [7] H. Liu, N. Han, and J. Zhao, Atomistic insight into the oxidation of monolayer transition metal dichalcogenides: From structures to electronic properties, *RSC Advances* **5**, 17572 (2015).
- [8] F. Hou, D. Zhang, P. Sharma, S. Singh, T. Wu, and J. Seidel, Oxidation Kinetics of WTe₂ Surfaces in Different Environments, *ACS Applied Electronic Materials* **2**, 2196 (2020).
- [9] C. R. Thomas, M. K. Vallon, M. G. Frith, H. Sezen, S. K. Kushwaha, R. J. Cava, J. Schwartz, and S. L. Bernasek, Surface Oxidation of Bi₂(Te,Se)₃ Topological Insulators Depends on Cleavage Accuracy, *Chemistry of Materials* **28**, 35 (2016).
- [10] P. F. Bagwell, Suppression of the Josephson current through a narrow, mesoscopic, semiconductor channel by a single impurity, *Physical Review B* **46**, 12573 (1992).
- [11] F. Schindler, A. M. Cook, M. G. Vergniory, Z. Wang, S. S. P. Parkin, B. A. Bernevig, and T. Neupert, Higher-order topological insulators, *Science Advances* **4**, eaat0346 (2018).
- [12] W. A. Benalcazar, B. A. Bernevig, and T. L. Hughes, Quantized electric multipole insulators, *Science* **357**, 61 (2017).
- [13] Z. Wang, B. J. Wieder, J. Li, B. Yan, and B. A. Bernevig, Higher-Order Topology, Monopole Nodal Lines, and the Origin of Large Fermi Arcs in Transition Metal Dichalcogenides XTe₂ (X = Mo, W), *Physical Review Letters* **123**, 186401 (2019).
- [14] L. Peng, Y. Yuan, G. Li, X. Yang, J. J. Xian, C. J. Yi, Y. G. Shi, and Y. S. Fu, Observation of topological states residing at step edges of WTe₂, *Nature Communications* **8**, 1 (2017).
- [15] C. Huang, A. Narayan, E. Zhang, X. Xie, L. Ai, S. Liu, C. Yi, Y. Shi, S. Sanvito, and F. Xiu, Edge superconductivity in multilayer WTe₂ Josephson junction, *National Science Review* **7**, 1468 (2020).
- [16] A. Kononov, M. Endres, G. Abulizi, K. Qu, J. Yan, D. G. Mandrus, K. Watanabe, T. Taniguchi, and C. Schönberger, Superconductivity in type-II Weyl-semimetal WTe₂ induced by a normal metal contact, *Journal of Applied Physics* **129**, 113903 (2021).
- [17] A. Kononov, G. Abulizi, K. Qu, J. Yan, J. Yan, D. Mandrus, D. Mandrus, K. Watanabe, T. Taniguchi, and C. Schönberger, One-Dimensional Edge Transport in Few-Layer WTe₂, *Nano Letters* **20**, 4228 (2020).
- [18] P. J. Zomer, M. H. Guimarães, J. C. Brant, N. Tombros, and B. J. Van Wees, Fast pick up technique for high quality heterostructures of bilayer graphene and hexagonal boron nitride, *Applied Physics Letters* **105**, 013101 (2014).
- [19] See Supplemental Material for detailed description of the fabrication process and additional EDX analysis.
- [20] P. Blake, E. W. Hill, A. H. Castro Neto, K. S. Novoselov, D. Jiang, R. Yang, T. J. Booth, and A. K. Geim, Making graphene visible, *Applied Physics Letters* **91**, 063124 (2007).
- [21] Y. Zhao, H. Liu, J. Yan, W. An, J. Liu, X. Zhang, H. Wang, Y. Liu, H. Jiang, Q. Li, Y. Wang, X. Z. Li, D. Mandrus, X. C. Xie, M. Pan, and J. Wang, Anisotropic magnetotransport and exotic longitudinal linear magnetoresistance in WTe₂ crystals, *Physical Review B - Condensed Matter and Materials Physics* **92**, 41104 (2015).
- [22] B. E. Brown, The crystal structures of WTe₂ and high-temperature MoTe₂, *Acta Crystallographica* **20**, 268 (1966).
- [23] T. R. Chang, S. Y. Xu, G. Chang, C. C. Lee, S. M. Huang, B. K. Wang, G. Bian, H. Zheng, D. S. Sanchez, I. Belopolski, N. Alidoust, M. Neupane, A. Bansil, H. T. Jeng, H. Lin, and M. Zahid Hasan, Prediction of an tunable Weyl Fermion metallic state in Mo_xW_{1-x}Te₂, *Nature Communications* **7**, 1 (2016).
- [24] A. Karki, D. Browne, S. Stadler, J. Li, and R. Jin, PdTe: A strongly coupled superconductor, *Journal of Physics: Condensed Matter* **24**, 055701 (2012).
- [25] B. Tiwari, R. Goyal, R. Jha, A. Dixit, and V. Awana, PdTe: a 4.5 K type-II BCS superconductor, *Superconductor Science and Technology* **28**, 055008 (2015).
- [26] S. Das, Amit, A. Sirohi, L. Yadav, S. Gayen, Y. Singh, and G. Sheet, Conventional superconductivity in the type-II Dirac semimetal PdTe₂, *Physical Review B* **97**, 14523 (2018).
- [27] J. A. Voerman, J. C. De Boer, T. Hashimoto, Y. Huang, C. Li, and A. Brinkman, Dominant s-wave superconducting gap in PdTe₂ observed by tunneling spectroscopy on side junctions, *Physical Review B* **99**, 14510 (2019).
- [28] Y. B. Choi, Y. Xie, C. Z. Chen, J. Park, S. B. Song, J. Yoon, B. J. Kim, T. Taniguchi, K. Watanabe, J. Kim, K. C. Fong, M. N. Ali, K. T. Law, and G. H. Lee, Evidence of higher-order topology in multilayer WTe₂ from Josephson coupling through anisotropic hinge states, *Nature Materials* **19**, 974 (2020).
- [29] M. R. Sinko, C. Sergio, O. Lanes, K. Watanabe, T. Taniguchi, S. Tan, D. Pekker, M. Hatridge, and B. M. Hunt, Superconducting contact and quantum interference between two-dimensional van der waals and three-dimensional conventional superconductors, *Physical Review Materials* **5**, 014001 (2021).
- [30] S. Ghatak, O. Breunig, F. Yang, Z. Wang, A. A. Taskin, and Y. Ando, Anomalous Fraunhofer patterns in gated Josephson junctions based on the bulk-insulating topological insulator BiSbTeSe₂, *Nano letters* **18**, 5124 (2018).
- [31] M. Tinkham, *Introduction to Superconductivity*, 2nd ed. (Dover Publications, 2004).
- [32] A. De Cecco, K. Le Calvez, B. Sacépé, C. B. Winkelmann, and H. Courtois, Interplay between electron overheating and ac Josephson effect, *Physical Review B* **93**, 180505 (2016).

- [33] H. Courtois, M. Meschke, J. Peltonen, and J. P. Pekola, Origin of hysteresis in a proximity Josephson junction, *Physical review letters* **101**, 067002 (2008).
- [34] A. Kononov, M. Endres, G. Abulizi, K. Qu, J. Yan, D. G. Mandrus, K. Watanabe, T. Taniguchi, and C. Schönberger, Superconductivity in type-II Weyl-semimetal WTe₂ induced by a normal metal contact, *Journal of Applied Physics* **129**, 113903 (2021).
- [35] P. Dubos, H. Courtois, B. Pannetier, F. Wilhelm, A. Zaikin, and G. Schön, Josephson critical current in a long mesoscopic SNS junction, *Physical Review B* **63**, 064502 (2001).
- [36] M. Bai, F. Yang, M. Luysberg, J. Feng, A. Bliesener, G. Lippertz, A. A. Taskin, J. Mayer, and Y. Ando, Novel self-epitaxy for inducing superconductivity in the topological insulator (Bi_{1-x}Sb_x)₂Te₃, *Phys. Rev. Materials* **4**, 094801 (2020).
- [37] M. Octavio, M. Tinkham, G. Blonder, and T. Klapwijk, Subharmonic energy-gap structure in superconducting constrictions, *Physical Review B* **27**, 6739 (1983).
- [38] K. Flensberg, J. B. Hansen, and M. Octavio, Subharmonic energy-gap structure in superconducting weak links, *Physical Review B* **38**, 8707 (1988).
- [39] F.-X. Xiang, A. Srinivasan, Z. Du, O. Klochan, S.-X. Dou, A. R. Hamilton, and X.-L. Wang, Thickness-dependent electronic structure in WTe₂ thin films, *Physical Review B* **98**, 035115 (2018).
- [40] A. Murani, A. Kasumov, S. Sengupta, Y. A. Kasumov, V. Volkov, I. Khodos, F. Brisset, R. Delagrèze, A. Chelianskii, R. Deblock, H. Bouchiat, and S. Guéron, Ballistic edge states in bismuth nanowires revealed by squid interferometry, *Nature Communications* **8**, 1 (2017).
- [41] L. Galletti, S. Charpentier, M. Iavarone, P. Lucignano, D. Massarotti, R. Arpaia, Y. Suzuki, K. Kadowaki, T. Bauch, A. Tagliacozzo, *et al.*, Influence of topological edge states on the properties of Al/Bi₂Se₃/Al hybrid Josephson devices, *Physical Review B* **89**, 134512 (2014).
- [42] M. Bai, X.-K. Wei, J. Feng, M. Luysberg, A. Bliesener, G. Lippertz, A. Uday, A. A. Taskin, J. Mayer, and Y. Ando, Proximity-induced superconductivity in (Bi_{1-x}Sb_x)₂Te₃ topological-insulator nanowires, *Communications Materials* **3**, 1 (2022).
- [43] M. Ohtomo, R. S. Deacon, M. Hosoda, N. Fushimi, H. Hosoi, M. D. Randle, M. Ohfuchi, K. Kawaguchi, K. Ishibashi, and S. Sato, Josephson junctions of Weyl semimetal WTe₂ induced by spontaneous nucleation of PdTe superconductor, *Applied Physics Express* **15**, 075003 (2022).

Supplementary Information: Transparent Josephson Junctions in Higher-Order Topological Insulator WTe_2 via Pd Diffusion

Martin Endres,¹ Artem Kononov,¹ Michael Stiefel,² Marcus Wyss,³
Hasitha Suriya Arachchige,⁴ Jiaqiang Yan,^{4,5} David Mandrus,^{6,4,5}
Kenji Watanabe,⁷ Takashi Taniguchi,⁷ and Christian Schönenberger^{1,3}

¹*Department of Physics, University of Basel,
Klingelbergstrasse 82, 4056 Basel, Switzerland*

²*Laboratory for Nanoscale Material Science,
Swiss Federal Laboratories for Material Science and Technology,
EMPA, Überlandstr. 129, 8600 Dübendorf, Switzerland*

³*Swiss Nanoscience Institute, University of Basel,
Klingelbergstrasse 82, 4056 Basel, Switzerland*

⁴*Department of Physics and Astronomy,
University of Tennessee, Knoxville, Tennessee 37996, USA*

⁵*Material Science and Technology Division,
Oak Ridge Laboratory, Oak Ridge, Tennessee 37831, USA*

⁶*Department of Materials Science and Engineering,
University of Tennessee, Knoxville, Tennessee 37996, USA*

⁷*National Institute for Materials Science,
1-1 Namiki, Tsukuba 305-0044, Japan*

(Dated: August 22, 2022)

MATERIALS AND METHODS

In the following section we outline the fabrication process of the samples shown in the main text. We highlight process steps that include heating of the device (!), which likely promotes the diffusion of Pd into the WTe_2 crystal.

1. Palladium bottom contacts.

- Standard e-beam evaporation of 3 nm titanium (Ti) and 15 nm* palladium (Pd) on p-doped Si/SiO₂ substrates.

* The thickness of Pd with 15 nm was found to provide good superconducting contact while at the same time ensures proper encapsulation of WTe_2 by hBN. A problem arising with increasing Pd thickness is that the covering hBN flake is not sealing off the area around the bottom contacts well enough, such that gaps open along the bottom contacts through which oxygen can enter and oxidize the WTe_2 flake.

- Lift-off in 50 °C acetone.

2. Exfoliation of hexagonal boron nitride (hBN).

- Mechanical exfoliation of hBN on a Si/SiO₂ wafer with 285 nm oxide using adhesive tape.
- Choosing clean flakes of appropriate size with a thickness between 10 nm and 30 nm according to optical contrast [1].

3. Exfoliation of WTe_2 in an inert N₂ atmosphere to avoid degradation [2–4]. Oxygen level inside the glovebox below < 1 ppm.

- Preparation of Si/SiO₂ substrates in an oxygen plasma at 30 W for 5 min. Quick transfer into the glovebox.
- Mechanical exfoliation of WTe_2 with an adhesive tape and transfer onto a polydimethylsiloxane (PDMS) stamp.
- PDMS stamp and Si/SiO₂ substrate are brought in contact.
- Heating of the package for 5 min at 120 °C and full cool-down for 15 min.
- Separation of the PDMS stamp and the substrates.

- Selection of elongated WTe_2 flakes along the crystallographic a-axis [5]. Desired thickness of the flakes ~ 10 nm to 30 nm.
4. Assembly of the vdW hetero-structure via the dry transfer technique [6].
- Fabrication of the polycarbonate (PC)/PDMS stamp.
 - Pick-up of the selected hBN and afterwards WTe_2 flakes at $T = 80^\circ\text{C}$.
 - Alignment of the stack with Pd bottom contacts and bringing in stack in contact.
 - !! Release of the PC/PDMS stamp from the stack by heating the package to 155°C for ~ 10 min.
 - Removal of remaining PC residues in dichloromethane for 1 h.
5. Contacting the stack: Depending on the transport experiment, contact to WTe_2 is either made through the Pd bottom contacts or through superconducting contacts made out of aluminium (Al) or molybdenum-rhenium (MoRe).
- !! Spin-coating the device with PMMA and successive bake-out at $T = 180^\circ\text{C}$ for 3 min.
 - Standard e-beam lithography to pattern the leads and bonding pads.
 - Normal Pd contacts:
 - e-beam evaporation of ~ 100 nm Au for the leads to contact the Pd bottom contacts.
 - Lift-off in 50°C acetone.
 - SC contacts:
 - CHF_3/O_2 plasma etching** in a RIE system to open up the top hBN.
- ** The etching process of the samples was calibrated such that the covering top hBN is safely removed and WTe_2 revealed underneath. Calibration of the etch rate for WTe_2 is more complex, as bare flakes oxidize and potentially behave differently compared to unoxidized flakes. For this reason, the remaining WTe_2 crystal on top of PdTe_x after etching varies slightly between the different samples, as can also be seen from comparison of figs. 2 a) with 3 a) in the main text.

Possibly, the MoRe contact could be separated from PdTe_x by a thin WTe_2 layer, forming an additional Josephson junction. However, in both curves, dV/dI and $V(I)$ in figs. 4 b) and 4 c) of the main text, we observe a zero resistance branch at low bias values. For this reason, the interface between the external contact and the sample does not contribute any parasitic resistance to the junction and a potential additional Josephson junction does not limit the performance of the sample or change the interpretation of the data.

- Transfer of the sample to the sputter machine. Ignition of an argon (Ar) plasma at 50 W for 1 min to clean the contact area.
- 100 nm thick sputtering of the superconducting leads and bond pads made out of Nb or MoRe.
- Lift-off in 50 °C acetone.

PD DIFFUSION DURING THE STACKING PROCESS

An open question remains when Pd diffuses from the bottom contact into the WTe_2 crystal on top. We have highlighted (!!) process steps during device fabrication that include heating and could facilitate the diffusion process. In the following we provide evidence that the diffusion of Pd into WTe_2 must happen already during the stacking process of the device.

Fig. S1 a) shows an optical image of the stack after the removal of PC but before etching and deposition of the superconducting contacts. The color change of hBN in between the Pd bottom contacts indicates that the WTe_2 flake is lifted off the bottom contacts at this stage. Fig. S1 b) presents a HAADF STEM image of the same stack, taken along a JJ. Visible are the two Pd bottom contacts at the left and right end of the image, with the WTe_2 spanning across them above. The WTe_2 flake is indeed lifted off the Pd bottom contacts, yet a PdTe_x diffusion layer has clearly formed inside the crystal. For this reason Pd must have diffused already during the stacking process, when the finished stack is being released on top of the bottom contacts and heated up to $T = 155\text{ °C}$ for ~ 10 min.

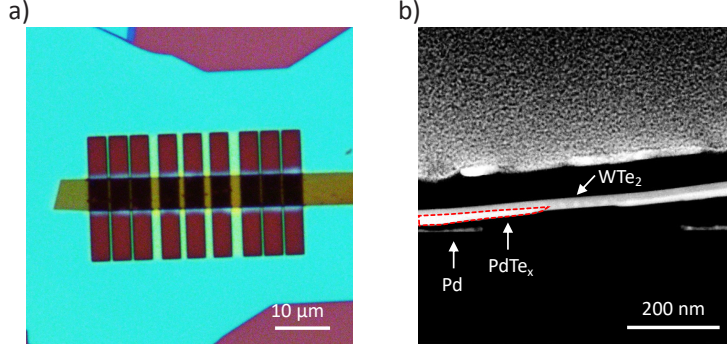


FIG. S1. **Diffusion of Pd during stacking process of the van der Waals (vdW) stack.**

a) Optical image of the finished vdW stack after PC removal. WTe_2 is lifted from the Pd bottom contacts, as seen by the color change of hBN in the large spacing between Pd bottom contacts.

b) HAADF image of the same device, showing the WTe_2 being lifted off the Pd bottom contacts. A swollen PdTe_x crystal structure has visibly formed inside the WTe_2 crystal, implying that Pd diffusion must happen already during the PC release at $T = 155^\circ\text{C}$ after the stacking process.

I. HORIZONTAL PD DIFFUSION IN THE REMAINING WTe_2

Figures S2 a) through d) present the HAADF image and the EDX spectra for W, Te and Pd of the WTe_2 crystal at the edge of the Pd bottom contact, which is indicated by white dashed lines. Figure S2 e) plots the atomic fraction in % in crystallographically unchanged WTe_2 , taken along the line cut indicated by the red arrow in fig. S2 a). The vertical dashed line in the plot indicates the extension of PdTe_x . Beyond this diffusion layer, the concentration of remaining Pd doping in WTe_2 decays close to zero within ~ 50 nm.

STEM AND EDX ANALYSIS

STEM and EDX analysis of Figs. 1 and 2 of the main text: The TEM-sample preparation has been carried out in a FEI Helios 660 G3 UC FIB/SEM-system. The preparation site was covered with a double layer of platinum in order to protect the layers of interest from any ion induced damage. The first Pt-layer was deposited by means of electron induced deposition at a beam energy of 3 keV and a beam current of 800 pA. This was followed by a second layer of Pt deposited by means of ion induced deposition at a beam energy of 30 keV and a beam current of 230 pA. The specimen cutting and polishing was carried out in the FIB at a beam energy of 30 keV and beam currents

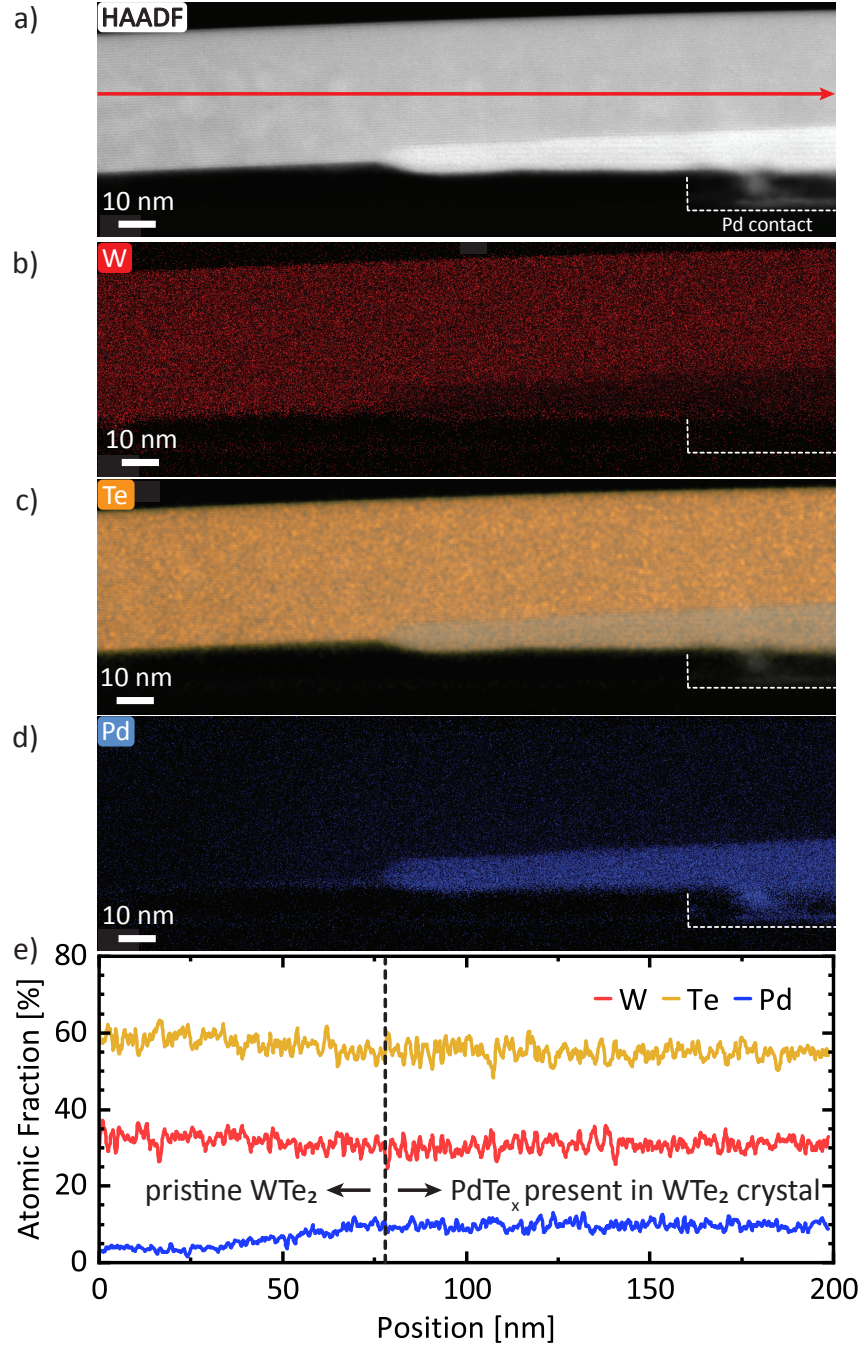


FIG. S2. **Horizontal diffusion of Pd inside the pristine WTe_2 crystal.** a) - d) HAADF image and EDX spectra for the elements W, Te and Pd. The extend of the former Pd bottom contact is outline by the white dashed line. e) Horizontal line-cut through the EDX spectra taken along the direction of red arrow in a) inside the pristine WTe_2 crystal above the PdTe_x layer. The extend of the PdTe_x layer is marked by a vertical dashed line. The diffused Pd concentration inside pristine WTe_2 decreases close to zero at ~ 50 nm beyond the PdTe_x diffusion layer.

ranging from 47 nA down to 80 pA. After reaching a sample thickness of <100 nm, the

sample was cleaned first at beam energies of 5 kV (beam current 41pA) and finally at 2 kV (beam current 23 pA). The transfer of the sample from the FIB to the TEM was carried out under argon atmosphere. The imaging of the TEM specimen was carried out in a FEI Titan Themis 3510. The machine was operated in the STEM-mode at a beam energy of 300 keV. The EDX data was post-processed using an average filter of six pixels (pre-filter) in the Velox software. The extracted EDS line scan data was further averaged over 50 neighbouring pixels for each measurement point.

STEM and EDX analysis of Fig. 3 of the main text: The TEM-sample preparation has been carried out in a FEI Helios NanoLab 650 DualBeam-system. The preparation of the lamella was similar to the already described preparation of Figs. 1 and 2. The imaging of the TEM specimen was carried out in a JEOL JEM-F200. The machine was operated in the STEM-mode at a beam energy of 200 kV. The EDX data were analyzed with the Analysis Station software, thereby the data has not been post-processed.

SAMPLE SPECIFICATIONS

Table S1 summarizes the samples used in the main text. In all samples, WTe₂ is placed Pd bottom contacts.

Sample	Appearance	d_{WTe_2} [nm]	d_{hBN} [nm]	SC contact, thickness of material
EDX EMPA	Fig. 1, 2	35.0	12.8	Nb, 100 nm
EDX 210317	Fig. 3 a)	23.0	53.0	MoRe, 100 nm
EDX 210805	Fig. 3 b)	~ 20*	~ 25*	No SC, contact through Pd bottom contacts
T 201022	Fig. 4 b), c)	21.9	24.5	MoRe, 80 nm
T Pd	Fig. 4 d)	~ 10*	~ 25*	No SC, contact through Pd bottom contacts

TABLE S1. Summary of samples used for the main text. Thickness values of the flakes were determined by AFM. Values highlighted by * were determined through the optical contrast of the flakes [1].

-
- [1] P. Blake, E. W. Hill, A. H. Castro Neto, K. S. Novoselov, D. Jiang, R. Yang, T. J. Booth, and A. K. Geim, Making graphene visible, [Applied Physics Letters](#) **91**, 063124 (2007).
- [2] H. Liu, N. Han, and J. Zhao, Atomistic insight into the oxidation of monolayer transition metal dichalcogenides: From structures to electronic properties, [RSC Advances](#) **5**, 17572 (2015).
- [3] F. Ye, J. Lee, J. Hu, Z. Mao, J. Wei, and P. X.-L. Feng, Environmental Instability and Degradation of Single- and Few-Layer WTe₂ Nanosheets in Ambient Conditions, [Small](#) **12**, 5802 (2016).
- [4] F. Hou, D. Zhang, P. Sharma, S. Singh, T. Wu, and J. Seidel, Oxidation Kinetics of WTe₂ Surfaces in Different Environments, [ACS Applied Electronic Materials](#) **2**, 2196 (2020).
- [5] Y. Zhao, H. Liu, J. Yan, W. An, J. Liu, X. Zhang, H. Wang, Y. Liu, H. Jiang, Q. Li, Y. Wang, X. Z. Li, D. Mandrus, X. C. Xie, M. Pan, and J. Wang, Anisotropic magnetotransport and exotic longitudinal linear magnetoresistance in WTe₂ crystals, [Physical Review B - Condensed Matter and Materials Physics](#) **92**, 41104 (2015).
- [6] P. J. Zomer, M. H. Guimarães, J. C. Brant, N. Tombros, and B. J. Van Wees, Fast pick up technique for high quality heterostructures of bilayer graphene and hexagonal boron nitride, [Applied Physics Letters](#) **105**, 013101 (2014).